On the Stability of Nonequilibrium Steady-States for the Electrode Processes at a Streaming Mercury Electrode

Marek Orlik* and Rafał Jurczakowski

Laboratory of Electroanalytical Chemistry, Department of Chemistry, University of Warsaw, ul. Pasteura 1, PL-02-093 Warsaw, Poland

Received: April 3, 2002

The streaming mercury electrode was found to be particularly useful for the study of the nonlinear dynamical phenomena (oscillations and multistability) in the electroreduction of pseudohalogenide complexes of nickel(II). Following our earlier experimental and simulation studies, we present the basic theoretical description of such instabilities. First, the steady states were found from the theory of electrode processes controlled by the rate of charge-transfer step, and the stability of these states was determined for the case when the electrode potential E was the only dynamical variable considered. The corresponding instability criterion was derived, which emphasized the role of the capacitive current, permanently charging the surface of the flowing mercury stream. For a further description of both bistability and oscillations in a two-dimensional variable space (electrode potential E - surface concentration of the reactant c_s) the existence of steady states was analyzed in terms of the dE/dt and dc_s/dt nullclines and the bifurcation diagram in the parameter space: (external voltage U − serial ohmic resistance R_s) was constructed. The dimensionless forms of derived equations were briefly discussed in terms of the different time scales for the dE/dt and dc_s/dt dynamics, what affects the shape of oscillations. Theoretical results were compared with the experimental data for the Ni(II)−SCN^- electroreduction.

1. Introduction

Electrochemical instabilities constitute a numerous class of nonlinear dynamical phenomena, the mathematical description of which reveals many similarities (universalities) with analogous processes in other, also nonelectrochemical systems.[1−4] However, electrochemical systems have their specific features which originate from the structure of the electrode/electrolyte interface, the mechanism of the charge-transfer step and the nature of the transport (diffusion, migration, convection) processes of the reactant from the bulk toward the reaction site at the interface. Therefore, if the theoretical description of nonlinear phenomena is intended to be compared directly with the real electrochemical process, as in the present paper, the mathematical dependencies must be based on the equations related strictly to all of these specific features of the experimental system.

Electrochemical instabilities, like periodic and chaotic current/potential oscillations, as well as the bistable behavior have been studied so far quite intensively on different types of electrodes, including dropping mercury electrode (DME), stationary (or static) mercury electrodes (SME), stationary and rotating disk (RDE) solid (e.g., Pt, Au, Ni, Fe, Sn) electrodes.[5,6] Of these electrode types, mercury is particularly suitable for processes which have to be investigated at relatively negative potentials, but using the dropping or static versions of such electrodes may not allow to study *true* steady-states or *sustained* oscillations. Of course, the diffusion to spherical electrodes should asymptotically attain the steady state, but one has to wait for it, simultaneously trying to diminish the effects of accidental convection. Furthermore, the accumulation of reaction products inside the small mercury drop and/or on its surface can induce a significant drift of such a state or even suppress the electrode process completely. Problems of this kind are typical, e.g., of the oscillatory electroreduction of the thiocyanate complexes of nickel(II).[7,8] Therefore, in our previous paper,[9] we described the construction and novel application of the *streaming* mercury electrode to the studies of the nonlinear dynamic instabilities associated with this process. For the Ni(II)−SCN^- electroreduction[9] we observed mainly bistability, as well as oscillations in a tiny region of control parameters: external voltage and serial resistance in the electric circuit. Recently, we applied our streaming electrode also to the studies of the electroreduction of azide complexes of nickel(II),[10] and we reported bistability and even tristability in its dynamical behavior. On the basis of these experimental results, supported with numerical simulations with the finite differences algorithm,[9,11,12] we came to the conclusion that the application of the streaming electrode to the studies of electrochemical instabilities is a proper and successful experimental solution of the problem of both the constant supply of the reactant and the removal of undesirable reaction products.

So far, in the theoretical parts of our studies,[7−10] we used mathematical dependencies derived from the classical theory of electrode processes,[13,14] for the case when their overall rate was controlled by the charge-transfer step, coupled with the reactant transport toward the electrode. Such electrochemical characteristics would, of course, be completely sufficient for the description of the course of the electrode processes, in which no nonlinear instabilities are observed. However, if current oscillations and multistability occur, then it is useful to extend the theoretical explanation of the system's behavior for the approach typical of the methods of nonlinear dynamics. In view of that, the main goal of our present paper is to analyze more

* To whom correspondence should be addressed. E-mail: morlik@chem.uw.edu.pl. Fax: +48 22 822 59 96. Phone +48 22 822 02 11 ext. 245.

10.1021/jp025885a CCC: $22.00
Published on Web 06/29/2002

generally the stability of steady-states for the electrode processes with negative differential resistance (NDR) in their current−voltage ($I-U$) characteristics, and studied at the streaming liquid electrode.

Numerical calculations were done in Pascal with the IBM PC and Unix machines. At every important step of our theoretical considerations, we made comparisons with the relevant experimental results for the electroreduction of the thiocyanate complexes of nickel(II), as the representative example of the analyzed oscillatory and bistable behaviors. The experimental setup, preparation of solution samples with Ni(II)−SCN^- complexes, and methodology of measurements with the streaming electrode were described in detail in our previous paper.[9]

2. Electrochemical Description of Steady-States at Streaming Electrodes

The electroreduction of the Ni(II)−SCN^- species can be satisfactorily described in terms of the apparently simple model process

$$\mathrm{Ox} + ne \underset{k_b}{\overset{k_f}{\rightleftharpoons}} \mathrm{Red} \tag{1}$$

but with such a dependence of rate constants k_f and k_b on the electrode potential E, which generates the NDR region on the current−potential relationship. For such a process, studied at the *streaming* electrode/solution interface the equivalent circuit shown in Figure 1 can be proposed. As usual, the total current I splits into (i) capacitive current I_c, associated with the charging of the double layer of the impedance Z_c and (ii) faradaic current I_f, flowing through the element of impedance Z_f which exhibits the NDR region in the $I-E$ characteristics. The reason for which a simple capacitor (as for the nonstreaming and nonporous electrodes) is here replaced by the complex element of the impedance Z_f (cf., Figure 1-A) is the *specific* feature of the *streaming* liquid electrode. While the nonstreaming electrodes experience the charging of the double layer only for relatively short time, until the imposed electrode potential (if constant) is attained, in our case the stream of fresh mercury, constantly flowing out at the glass capillary tip, needs a *permanent charging*, even if the desired electric potential is kept perfectly constant and no any faradaic process occurs. This situation is to some extent analogous to the permanent charging of the classical dropping mercury electrode (DME) which however does not offer the possibility to study any true-steady states or sustained oscillations, due to the overlapping effects of the pulsating changes of the electrode surface.

Thus, the charge-balance eq 2 for the *unperturbed* electrochemical steady-state (ss) at the streaming electrode must include the contribution, to the overall current I, from the *steady-state capacitive current* $I_{c,ss}$

$$I_{ss} = \frac{U - E_{ss}}{R_s} = I_{f,ss} + I_{c,ss} \tag{2}$$

where

$$I_{c,ss} = \frac{\mathrm{d}Q_{dl}}{\mathrm{d}t} = \frac{\mathrm{d}\{\, C_d A(t)[E_{ss} - E_{pzc}]\}}{\mathrm{d}t} = 2\pi r C_d (E_{ss} - E_{pzc})v \tag{3}$$

In eqs 2 and 3, U is the external voltage applied, E_{ss} is the steady-state interfacial potential drop, R_s is the serial ohmic resistance (cf., Figure 1), Q_{dl} is the the double layer charge, C_d is the double layer capacity (per unit area), E_{pzc} is the potential of zero charge, $A = 2\pi rl$ is the surface area of the mercury stream of a length l and radius r, and $v = \mathrm{d}l/\mathrm{d}t$ is a mercury stream velocity. Formally, relationship 3 can be also expressed as the ratio of the voltage E_{ss} *decreased* by the value E_{pzc} and applied to the ohmic resistance R_d

$$I_{c,ss} = \frac{E_{ss} - E_{pzc}}{R_d} \tag{4}$$

where R_d is defined by

$$R_d = \frac{1}{2\pi r C_d v} \tag{5}$$

and called by us here a "zero frequency capacitive resistance". In Figure 1-B (see the area framed by the dotted rectangle), we suggest the electronic interpretation of Z_f from Figure 1-A, which meets the relationship 4: the potential difference E applied to the constant ohmic resistance R_d is decreased by the electromotive force E_{pzc} of the virtual galvanic cell connected in series, with a proper electrode polarization for such compensation. Alternatively, one can consider a circuit without this virtual cell, but then the full interfacial potential drop E has to be applied to the potential-dependent resistance, equal then to $R_d = E/[2\pi r C_d v(E - E_{pzc})]$. Independently of the particular

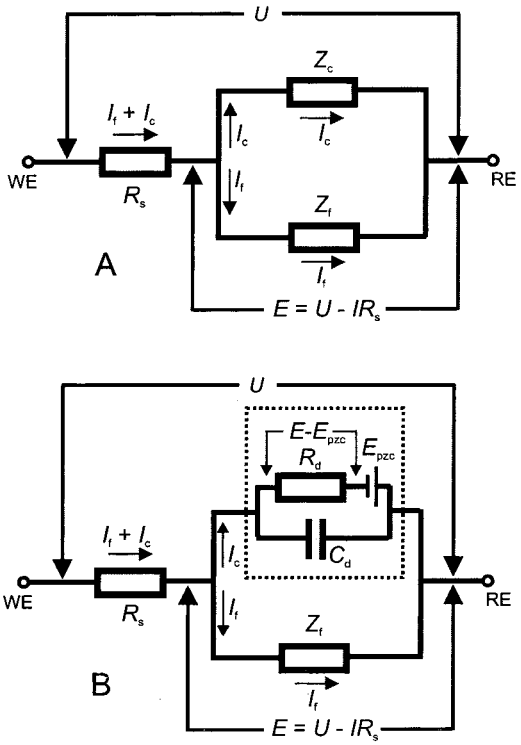

Figure 1. (A) General equivalent circuit for the electrode process occurring at the streaming mercury electrode, represented by the parallel connection of the elements of the impedance Z_f and Z_c, associated with the flow of the faradaic I_f and capacitive I_c currents, respectively. The capacitive current I_c flows through the element of impedance Z_c even at the steady-state potential E_{ss} and in the absence of the faradaic process. (B) The equivalent circuit from Figure A extended for the exemplary equivalent sub-circuit (in dotted rectangle) for the complex element of an impedance Z_c: in the steady-state the capacitive current flows through the resistor $R_d = (2\pi r C_d v)^{-1}$ to which the electrode potential E, decreased for the electromotive force E_{pzc}, is applied; r − radius of the mercury stream, flowing with the velocity v (see text for a more detailed description).

formal concept, the final expression for the capacitive current will reduce to eq 4. In further considerations we shall keep the concept of resistance R_d, given by eqs 4 and 5, corresponding to the construction of the equivalent circuit from Figure 1-B.

In the absence of serial ohmic resistance R_s (ohmic potential drop) the total faradaic current I_f at the streaming electrode is the steady-state current $I_{f,ss}$, achieved due to the constant rate of the mixed convective-diffusion transport of the reactant toward the electrode surface. The expression for such a current can be derived analytically from the integration, along the entire stream length $(0,...l_{max})$, of the partial faradaic currents flowing through the $dA = 2\pi r dl$ element of the mercury stream[10,15]

$$I_{f,ss} = -2\pi r n F c_{ox}^0 k_f v \left[\frac{2}{\kappa}\sqrt{\frac{t_{max}}{\pi}} + \frac{\exp(\kappa^2 t_{max})\mathrm{erfc}(\kappa t_{max}^{1/2}) - 1}{\kappa^2}\right] \quad (6)$$

where n is the number of electrons involved in the electrode process (1) (here $n = 2$, as for the Ni(II)−SCN^- electroreduction), F is Faraday's constant, c_{ox}^0 is the bulk concentration of the reducible reactant, $t_{max} = l_{max}/v$ − is the maximum time of contact of the electrolyzed solution with the mercury surface (attained at the end l_{max} of the mercury stream), kinetic parameter $\kappa = (k_f/D_{ox}^{1/2} + k_b/D_{red}^{1/2})$, with D's − the diffusion coefficients of the corresponding species, and the minus at the beginning of the whole formula 6 makes the value of the reduction current algebraically negative, according to the presently recommended convention.

For the electrochemical kinetic characteristics of the Ni(II)−SCN^- electroreduction, we refer to our previously[9] applied experimental conditions and the determined dependence of the rate constant k_f on the electrode potential E

$$k_f = k_{s,1}^{app}\left\{\frac{1}{1+\exp[P_1(E-P_2)]}\right\}\exp[-(\alpha n)_1 f(E-E_f^0)] + k_{s,2}^{app}\exp[-(\alpha n)_2 f(E-E_f^0)] \quad (7)$$

where $k_{s,1}^{app} = 1 \times 10^{-3}$ cm s^{-1}, $k_{s,2}^{app} = 4 \times 10^{-4}$ cm s^{-1}, $(\alpha n)_1 = 1.50$, $(\alpha n)_2 = 0.12$, $E_f^0 = -0.662$ V, $P_1 = -67.4$ V^{-1}, $P_2 = -0.798$ V, and $f = F/RT$ (with $T = 298.15$ K).

Thus, if a serial resistance R_s in the electric circuit is equal to zero, using eqs 3, 6, and 7 one can directly calculate the theoretical faradaic $I_{f,ss}$ and capacitive $I_{c,ss}$ steady-state currents for such a condition (see Figure 2-A). Some discrepancies between the courses of the experimental and theoretical total current $I = I_{f,ss} + I_{c,ss}$ vs. E, observed particularly at far negative potentials, originate presumably from the simplifying assumption on the potential-independent (average) double layer capacity $C_d = 26.7$ μF cm^{-2} (cf., refs 8,9) and from some imperfections of the real streaming electrode,[15,16] idealized for our theoretical considerations, as done and discussed by us also previously.[9]

If the serial resistance R_s is greater than zero, the analogous calculation involving eqs 3, 6, and 7 is based on the *iterative* numerical search for I_f and I_c for given U and R_s, according to the procedure described in detail in ref 10. For conditions when experimentally bistability (hysteresis) is observed, such calculations lead to the full folded diagram of the stable and unstable steady states, quite well concordant with the experimental points, as Figure 2-B proves. This method of calculation is much faster and yields the folded shape much better concordant with the experimentally determined characteristics of stable steady-states than the fold determined previously from the numerical simulation based on a simplified (averaged over the electrode length) expression for the faradaic current (cf. Figure 10 in ref 9). However, the previously published algorithm still remains particularly useful for the *realistic* model reproduction of the hysteresis observed experimentally in the current response to the potentiodynamic (cyclic) changes of the external voltage within the bistable region (cf., Figure 9 in ref 9).

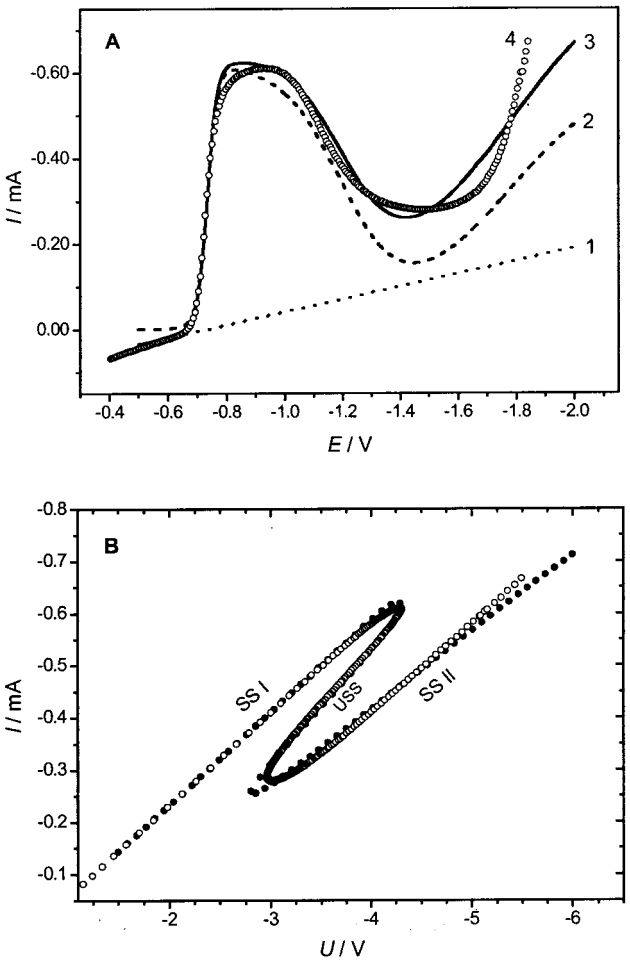

Figure 2. (A) Collection of the calculated steady-state: (1) capacitive $I_{c,ss}$ (eq 3), (2) faradaic $I_{f,ss}$ (eq 6), and (3) total ($I = I_{f,ss} + I_{c,ss}$) currents for the Ni(II)−SCN^- electroreduction at the streaming electrode, compared with the experimental points[9] (4, ○) for the same conditions, with serial resistance $R_s = 0$ and constant (averaged) double layer capacity $C_d = 26.7$ μF cm^{-2}; (B) (●) the corresponding full diagram of the stable (SS I, SS II) and unstable (USS) steady-states calculated iteratively from eqs 3, 6, and 7 for the serial resistance $R_s = 5.5$ kΩ (for mathematical details see ref 10, compared with data obtained from the experiment (○).[9] Composition of the sample: 5.0 mmol dm^{-3} Ni$(ClO_4)_2$ + 2.0 mol dm^{-3} NaSCN. Parameters of the streaming electrode: capillary flow $m = 210$ mg s^{-1}, internal glass capillary (= mercury electrode) diameter $\phi = 0.11$ mm, length of mercury jet (directed upward) $l_{max} = 2.5$ mm. Temperature 298.0 K.

3. One-Dimensional Stability Analysis of the Steady-States at the Streaming Electrode

3.1. Differential Equation for the One-Dimensional Analysis. As long as only bistability (and not oscillations) is concerned, it is sufficient to analyze the stability of steady-states in terms of the electrode potential E as the only dynamical variable. For this purpose, one has to find conditions for which small *perturbations* (δE) of the steady-state electrode potential undergo either damping or amplification as a function of time, thus indicating the (asymptotic) stability or instability of the

state considered, respectively. Because this perturbation causes the recharging of a double-layer at a whole electrode surface ($2\pi r l_{max}$) (as also for the nonstreaming electrodes), eq 3 which described the capacitive current in the steady-state only, has now to be *extended* for the contribution proportional to dE/dt

$$I_c = \frac{dQ_{dl}}{dt} = \frac{d\{C_d A(t)[E(t) - E_{pzc}]\}}{dt} = 2\pi r C_d (E - E_{pzc})\upsilon + 2\pi r C_d l_{max}\left(\frac{dE}{dt}\right) \quad (8)$$

Combination of eq 8 with the charge balance condition (eq 2) applied now for any potential E leads to the formula for the dynamics of dE/dt as a function of E, with U and R_s treated as parameters

$$\frac{dE}{dt} = \frac{U - E}{2\pi r R_s C_d l_{max}} - \frac{(E - E_{pzc})\upsilon}{l_{max}} - \frac{I_f(E)}{2\pi r C_d l_{max}} \quad (9)$$

This dependence will serve further as the basis for different variants of the one-dimensional stability analysis of the steady-states at the streaming electrodes.

3.2 Dynamics of the Electrode Potential in Terms of the dE/dt = $f(E)$ Dependence. In the first step of our analysis, we focus on the full analytical expression for the dE/dt dynamics which is obtained from eq 9 by substitution of the eq 6 for the faradaic current

$$\frac{dE}{dt} = \frac{U - E}{2\pi r R_s C_d l_{max}} - \frac{(E - E_{pzc})\upsilon}{l_{max}} + \frac{nFc^0_{ox}\, k_f \upsilon\left[\frac{2}{\kappa}\sqrt{\frac{t_{max}}{\pi}} + \frac{\exp(\kappa^2 t_{max})\mathrm{erfc}(\kappa t_{max}^{1/2}) - 1}{\kappa^2}\right]}{C_d l_{max}} \quad (10)$$

For given U and R_s control parameters, this dependence allows us to find the possible steady-states (defined through the dE/dt = 0 condition) and to diagnose their *stability*. For parameters established from our experimental characteristics of the Ni(II)−SCN^- electroreduction (cf., eq 7 and caption to Figure 2) we constructed the dependencies of dE/dt on the electrode potential E for the constant serial resistance R_s = 5.5 kΩ and three exemplary values of the external voltage U: −2, −3.5, and −5 V (minus sign means that the streaming electrode was externally polarized negatively with respect to the reference electrode and the same convention will be used further for the sign of the electrode potential E). The curves obtained in this way are shown in Figure 3.

Let us consider in more detail the curve for U = −3.5 V. Three steady-states are possible for this control parameter. On the basis of the *sign* of dE/dt around the close vicinity of a given steady-state, it is easy to understand that the two extreme states are stable: the perturbations in their close neighborhood are damped as a function of time since for $E > E_{ss}$ the derivative dE/dt < 0 and the opposite tendency is true for $E < E_{ss}$. The middle steady-state is unstable (so impossible to observe experimentally), since local perturbations are amplified: dE/dt <0 for $E < E_{ss}$ and dE/dt >0 for $E > E_{ss}$. Obviously, the case considered corresponds to bistability that is indeed observed for the same (U, R_s) control parameters in the real experiment (cf., Figure 3 in ref 9). The above simple diagnosis of the stability of steady-states can be expressed also in terms of the formalism of the one-dimensional linear stability analysis.[17−20]

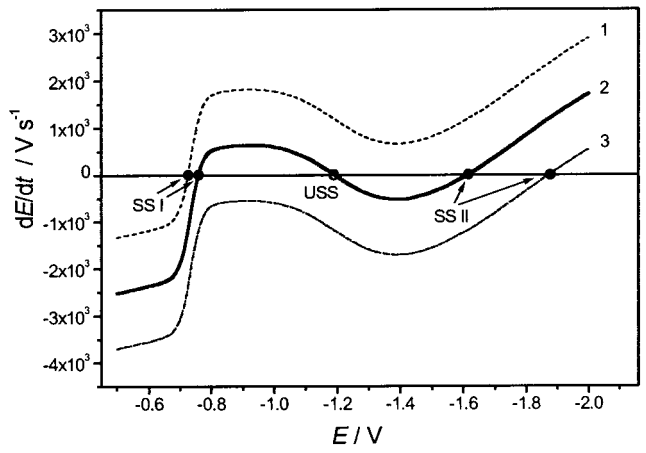

Figure 3. Theoretical characteristics of the system's dynamics (dE/dt) around the steady states (dE/dt = 0), obtained from eq 10 for the Ni(II)−SCN^- electroreduction at a streaming mercury electrode, for the serial ohmic resistance R_s = 5.5 kΩ and three exemplary values of the external voltage: (1) U = −2.0 V (monostability, state SS I), (2) U = −3.5 V (bistability: two extreme stable states: SS I, SS II, and one medium, unstable state USS); (3) U = −5 V (monostability, state SS II). Composition of the sample and other parameters − the same as for Figure 2 and in eq 7. The arrows show the evolution of local perturbations which, in dependence of the slope Θ = d[dE/dt]/dE in the close vicinity to the given steady-state value E_{ss}, determines its stability (Θ < 0) or instability (Θ > 0).

The Taylor series expansion of dE/dt around the small vicinity of a given steady-state E_{ss} may be limited to the linear term

$$\frac{dE}{dt} \equiv f(E) \cong f(E_{ss}) + \left.\frac{df}{dE}\right|_{E_{ss}} (E - E_{ss}) \quad (11\text{-A})$$

or, alternatively

$$\frac{d(\delta E)}{dt} = \Theta \times (\delta E) \quad (11\text{-B})$$

where $f(E_{ss})$ = 0 from the definition of the steady-state, Θ = $[df/dE]_{ss}$ and the small perturbation δE of the steady-state potential E_{ss} is defined through

$$\delta E = E - E_{ss} \quad (12)$$

Accordingly, Θ > 0 means the exponential growth, whereas Θ < 0 − the analogous decay of the perturbation δE what unambiguously indicates the instability or stability, respectively, of the steady-state potential in dependence on the d[dE/dt]/dE value.

For the verification of this first simple step of the theory, it is now useful to compare its predictions with our experimental data. The steady-state electrode potentials predicted by Figure 3 are reasonably well concordant with those found from our experiments[9] (obtained from the $E_{ss} = U - I_{ss}R_s$ recalculation). For the curve (1) in Figure 3: theoretical E_{ss} = −0.730 V, experimental value = −0.720 V; for curve (2) theoretical E_{ss} (1) = −0.757 V, E_{ss} (2) = −1.188 V, E_{ss} (3) = −1.612 V, experimental values = −0.758 V, −1.135 V, and −1.674 V, respectively; for curve (3) theoretical E_{ss} = −1.872 V, experimental value = −1.810 V. Taking into account some discrepancies between the experimental and theoretical currents (cf., Figure 2-A) which seem to be a main source of actually reported small differences in steady-state potentials, we think that the basic concept of the one-dimensional stability analysis of steady-states at the streaming electrodes is valid.

Finally, from the point of view of the formalism of nonlinear dynamics the consecutive curves shown in Figure 3 illustrate qualitatively different (monostable, bistable, monostable) behaviors, the transitions between which correspond to the (degenerate case) of the saddle-node bifurcations, associated with the creation and annihilation of the steady-states.

3.3. Instability Criterion of the Steady-State. A further analysis of the time evolution of the perturbation of the electrode potential E leads to the specific *instability condition* for the electric circuit from Figure 1. For the nonstreaming electrodes and processes with the NDR region such an instability condition is well established in the literature of electrochemical instabilities (cf. e.g., refs 5, 6, 21, and 22) and postulates the necessity of existence of negative faradaic impedance $Z_f < 0$ and serial resistance $R_s > -Z_f$. However, in our case the permanent flow of the capacitive current at a streaming electrode, even at the steady-state, as explained above, is a cause for the substantial modification of this condition.

An appropriate variant of the linear stability analysis, similarly as for the nonstreaming electrodes,[22] invokes again the small perturbation (δE) of the steady-state electrode potential E_{ss} (cf., equation 12) and, accordingly, assumes that the faradaic current flowing at any potential E close to E_{ss} may be approximated by the linear term of the Taylor series expansion of I_f around this steady-state

$$I_f(E) = I_f(E_{ss} + \delta E) = I_f(E_{ss}) + \left(\frac{dI_f}{dE}\right)_{ss} \delta E \qquad (13)$$

In eq 13 $(dE/dI_f)_{ss}$ is the zero-frequency faradaic impedance Z_f at the steady-state considered. The expression for the steady-state faradaic current $I_f(E_{ss})$ follows from eq 9 with $dE/dt = 0$ (or alternatively from eqs 2 and 3)

$$I_{f,ss} \equiv I_f(E_{ss}) = \frac{U - E_{ss}}{R_s} - 2\pi r C_d (E_{ss} - E_{pzc})\upsilon \qquad (14)$$

Substitution of eqs 12, 13, and 14 into eq 9 leads to the following relationship for the time evolution of perturbation

$$\frac{d(\delta E)}{dt} = -\frac{\delta E}{2\pi r C_d l_{max}}\left[\frac{1}{R_s} + \frac{1}{Z_f} + 2\pi r C_d \upsilon\right] \qquad (15)$$

which means that the steady-state *loses* its stability (i.e., $d(\delta E)/dt > 0$) when the expression in brackets attains a negative value

$$\frac{1}{R_s} + \frac{1}{Z_f} + 2\pi r C_d \upsilon < 0 \qquad (16)$$

or, alternatively, using the definition of the resistance R_d given by eq 5, when

$$\frac{1}{R_s} + \frac{1}{Z_f} + \frac{1}{R_d} < 0 \qquad (17)$$

Equation 16 is a searched instability condition for the steady-states at the streaming electrodes. Analysis of the physical sense of this inequality leads to the following further conclusions: (i) because R_s and R_d values can be only positive, the zero-frequency faradaic impedance Z_f must be negative; thereby for the stream velocity $\upsilon = 0$ the instability condition (16) obviously simplifies to that for the nonstreaming electrodes; (ii) for the process with a given negative faradaic impedance Z_f, the destabilization of the steady-state at the streaming electrode requires the serial ohmic resistance to meet the condition

$$R_s > \frac{1}{\left(-\frac{1}{Z_f}\right) - 2\pi r C_d \upsilon} = \frac{1}{\left(-\frac{1}{Z_f}\right) - \left(\frac{1}{R_d}\right)} > 0 \qquad (18)$$

which means that this resistance appears to be *higher* than for the analogous characteristics of the charge-transfer step at the nonstreaming electrode. The physical sense of this modification is the following: at the streaming electrode, due to the permanent contribution from the constantly flowing capacitive current to the overall current, the *net* current−potential characteristics of the electrochemical cell exhibit a *less* negative slope $dI/dE = d(I_f + I_c)/dE$ (i.e., *more negative* net polarization resistance dE/dI) than for the faradaic process alone: dI_f/dE (cf., curves 2 and 3 in Figure 2-A). Therefore, one has to apply the serial resistance appropriately, i.e., for the value $dE/dI_c = (2\pi r C_d \upsilon)^{-1}$ higher than in the absence of the steady-state current $I_{c,ss}$. From the comparison of the instability condition for the nonstreaming electrode with eq 18 it follows that the term $[(-1/Z_f) - 2\pi r C_d \upsilon]^{-1}$ in the latter relationship has a sense of this net slope of the dE/dI characteristics, to which the minimum value of R_s has to be actually adjusted. This again emphasizes the substantial role of the steady-state capacitive current in the stability characteristics of the electrode processes at the streaming liquid electrode, that does not manifest itself for other types of electrodes.

(iii) according to eq 18 the serial resistance R_s that ensures the onset of instability exists (i.e. is greater than zero) if the stream velocity υ meets the condition

$$0 < \upsilon < \left(\frac{-1}{2\pi r C_d Z_f}\right) \qquad (19)$$

This means that the instability will *not* be observed for too high values of υ, so a certain *optimum* stream velocity interval has to be chosen for the destabilization of the steady-state. The physical sense of this condition is the following: if the increasing stream velocity attains a critical value $\upsilon_{crit} = -(2\pi r C_d Z_f)^{-1}$ the contribution of the capacitive current totally compensates the negative zero-frequency impedance of the faradaic process and the net I vs E dependence becomes flat. Formally, then the *net* negative resistance of the I-E characteristics attains infinity and thus also infinite value of R_s would be necessary for the onset of instability. As long as the stream velocity is low enough and this compensation does not occur, there are still finite values of R_s possible for the fulfillment of the condition (18).

For comparison of the instability condition in the form of eq 18 with the experimental observations one should take into account that its derivation was based on the equivalent circuit (Figure 1) with the *N*-shaped NDR element, without performing any explicit considerations on the role of transport of electroactive species toward the electrode, which factor is particularly important for the onset and characteristics of oscillations. In other words, as mentioned at the beginning of this analysis, the equivalent circuit from Figure 1 can explain only the mono- or bistable (trigger-like) behavior, and therefore, criterion (18) can be compared only with the same types of behavior in the real system. Accordingly, from the course of the $I-E$ characteristics for the $Ni(II)-SCN^-$ electroreduction (cf., Figure 2 in ref 9) one can assess the minimum absolute value of the negative resistance as equal to ca. 800 Ω while the experimental bifurcation diagram (Figure 4 in ref 9) shows bistability starting

from R_s close to ca. 900 Ω (more precise assessment is difficult due to partial overlapping of the cusp of the monostable/bistable transition points with the oscillatory region). This result is however at least a semiquantitative confirmation of the validity of the instability condition for the streaming electrode, expressed by eqs 16 or 18.

4. Two-Dimensional Stability Analysis of the Steady-States at the Streaming Electrode

4.1. Differential Equations of the System's Dynamics. For the theoretical description of both bistability and oscillations in terms of the appropriate bifurcations, it is necessary to perform the stability analysis with more than one dynamical variable considered. Because in our experiments we did not observe chaos, the description of which would require the system of at least three (ordinary) differential equations, we limit the present theoretical analysis to a two-dimensional space, defined by the dynamical variables: interfacial potential drop $E(t)$ and the concentration of the reactant at the electrode surface $c_{ox}(x = 0,t)$ (or, more precisely, at the reaction site for which the coordinate $x = 0$ is assumed). Accordingly, the system of two ordinary differential equations is considered, which describes the evolution of perturbations of these dynamical variables as a function of time.

For a significant simplification of the mathematical treatment of this problem some assumptions, justified by the electrochemical characteristics of the experimental system, will be made. According to the first assumption, the region of a negative differential faradaic resistance is located at the potentials (with respect to the formal potential of the (Ni(II)-SCN^-/Ni(Hg) couple:[9] $E_f^0 = -0.662$ V) negative enough to neglect the contribution, to the faradaic current, of the (reverse) oxidation process Red → Ox; thus, we put $k_b = 0$ in eq 1)). Then the cathodic (algebraically negative) faradaic current may be expressed in terms of the surface concentration of Ox species only: $I_f = -nFAk_f c_{ox}(0,t)$, where $A = 2\pi r l_{max}$ is the total electrode surface area. Accordingly, the first differential equation, which can be considered the simplified version of eq 9, takes the form

$$\frac{dE}{dt} = \frac{U - E}{2\pi r R_s C_d l_{max}} - \frac{(E - E_{pzc})\upsilon}{l_{max}} + \frac{nFk_f c_{ox}(0,t)}{C_d} \equiv F[E, c_{ox}(0,t)] \quad (20)$$

The second differential equation which describes the $dc_{ox}(0,t)/dt$ dynamics follows from the general Fick's law ($\partial c/\partial t = -\mathrm{div}\vec{\mathbf{f}}$), where $\vec{\mathbf{f}}$ is (here) the diffusion flux of matter. Thereby, we invoke the second simplifying assumption which postulates the practically linear and one-dimensional (in the direction x normal to the electrode surface) character of this diffusion, what reduces the general Fick's law to the one-dimensional form: $\partial c/\partial t = -\,df_x/dx$. The third simplifying assumption postulates that the diffusion concentration profile of Ox species may be approximated by a linear shape which expands toward the bulk of the solution over the distance δ_N, i.e., the thickness of the Nernst diffusion layer. Two latter assumptions, suggested already by Koryta[23] and verified also in our numerical modelings[9] result from the extremely short electrolysis time (1−2 ms) for which the strict cylindrical geometry of diffusion practically does not manifest itself, and the role of concentration gradients along the electrode surface for the transport in this (y) direction can be neglected. The differential equation $dc_{ox}(0,t)/dt$ corresponding to the above assumptions has a form

$$\frac{dc_{ox}(0,t)}{dt} = -\frac{2k_f c_{ox}(0,t)}{\delta_N} + \frac{2D_{ox}[c_{ox}^0 - c_{ox}(0,t)]}{\delta_N^2} \equiv G[E, c_{ox}(0,t)] \quad (21)$$

which can be derived e.g. in a way shown by Koper and Sluyters.[24]

However, in the case of the streaming electrode this *single* Equation 21 describes the $dc_{ox}(0,t)/dt$ dynamics only at the *single selected* electrode site of the coordinate $y = l$, for which the y-dependent electrolysis time is equal to $t = l/\upsilon$ and, accordingly, the Nernst diffusion layer thickness may be approximated as $\delta_N = [\pi D t(l)]^{1/2}$ (strictly valid only for purely diffusion-controlled conditions). This means a mathematical complication of the problem which however can be satisfactorily simplified if, in the model, we replace the real streaming electrode with its virtual equivalent of the same *mean* residence time $\bar{t}_{res}$ and the associated *mean* diffusion layer thickness $\bar{\delta}_N$. The value of the latter quantity can be determined from the simple averaging formula

$$\bar{\delta}_N = (1/t_{max})\int_0^{t_{max}} \delta(t)dt = [(\pi D_{ox})^{1/2}/t_{max}]\int_0^{t_{max}} t^{1/2}dt = 2(\pi D_{ox} t_{max})^{1/2}/3 = 1.21\ \mu m \quad (22)$$

This result, confronted with our numerical simulations of the *realistic* concentration profiles in the bistable region of the Ni(II)−SCN^- electroreduction, made now according to our previously published procedure,[9] showed that the value of δ_N varied typically from 1.144 to 1.274 μm in the bistable region (see Figure 4), what confirms the above analytical assessment of $\bar{\delta}_N$. Accordingly, the value $\bar{\delta}_N = 1.2$ μm was accepted for all further calculations.

Nevertheless, one should remember that the approximation expressed by eq 21 with constant $\bar{\delta}_N$ (22) for the always linear concentration profile may be a source of some discrepancies between theoretical predictions and experimental results, particularly for oscillations, for which the nonlinear shape of the varying, time-dependent concentration profile can be important for their exact quantitative (period and amplitude) reproduction.

4.2. Steady-States in the Nullcline Representation. The mathematical conditions for the nullclines $dE/dt=0$ and $dc_{ox}(0,t)/dt = 0$, applied to eqs 20 and 21 with $\delta_N = \bar{\delta}_N$, lead to the following dependencies, in which (and, for simplicity, always so from here) we shall use the abbreviated symbol c_s for the variable $c_{ox}(0,t)$

$$dE/dt\ \textit{nullcline}:\ c_s = \frac{1}{nFk_f(E)l_{max}}\left[C_d\upsilon(E - E_{pzc}) - \frac{U - E}{2\pi r R_s}\right] \quad (23)$$

$$dc_s/dt\ \textit{nullcline}:\ c_s = \frac{c_{ox}^0}{1 + \dfrac{k_f(E)\bar{\delta}_N}{D_{ox}}} \quad (24)$$

The exemplary and representative courses of nullclines (23, 24) corresponding to the characteristics of the Ni(II)-SCN^- system, for the four various combinations of control parameters: U and R_s, are shown in Figure 5.

The intersection points of these nullclines correspond to the steady-states, and the signs of the $[dE/dt, dc_s/dt]$ values in the neighboring regions indicate the direction of the local evolution

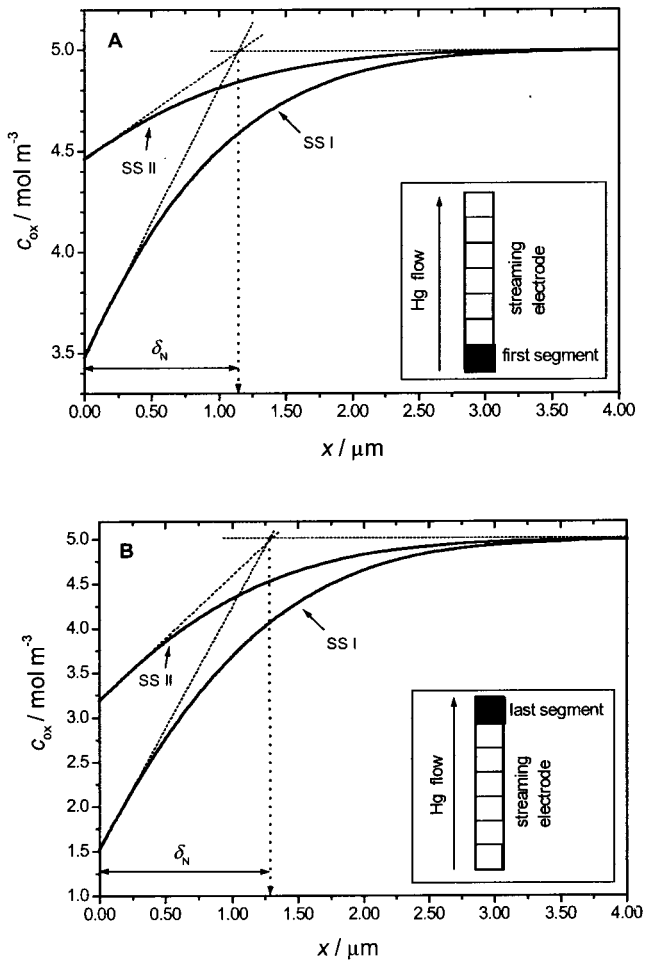

Figure 4. Exemplary simulated realistic concentration profiles for the electroreduction of Ox (Ni(II)−SCN$^-$ complex) in the bistable region ($U = -3.5$ V, $R_s = 5.5$ kΩ) for: (A) the first and (B) the last discrete segment of a model streaming mercury electrode, shown schematically in the insets. For the full discretization scheme and other mathematical details of the simulation procedure, see ref 9. Other model parameters, the same as for Figure 2.

of E and c_s variables as a function of time, what determines the stability of the steady-state considered. These four pictures correspond to the following: (A) monostability with respect to SS I state, (B) monostability with respect to SS II state, (C) SS I + SS II bistability with the unstable middle steady-state USS, (D) unstable single steady-state USS coexisting with stable sustained oscillations. For the latter case, the corresponding closed attracting phase trajectory (stable limit cycle), surrounding this unstable fixed point, was computed from the numerical integration of the equation system 20 and 21 by the fourth-order Runge−Kutta method with an automatic step size correction.[25]

Comparison of conclusions drawn from these nullclines with the experimental stability diagram of the Ni(II)−SCN$^-$ electroreduction (cf., Figure 4 in ref 9 or Figure 6-B below) shows that for the four sets of (U, R_s) parameters, considered in Figure 5, the same types of dynamic behavior were observed in a real experiment. Furthermore, the steady-state potentials from Figure 5-c: (−0.776 V, −1.172 V, −1.578 V) are reasonably close to the experimentally obtained values: (−0.770 V, −1.140 V, −1.670 V), respectively (with slight discrepancies presumably caused by the accumulation of all inaccuracies in fitting experimental curves and simplifications in the theoretical model). In our opinion, this confirms the validity of the model eqs 20 and 21 and of the proper choice of $\bar{\delta}_N$.

4.3. Linear Stability Analysis and the Bifurcation Diagram. For the analysis of the stability of steady-states the original differential eqs 20 and 21 were transformed to their linearized forms, in the matrix notation

$$\begin{bmatrix} \dfrac{d(\delta E)}{dt} \\ \dfrac{d(\delta c)}{dt} \end{bmatrix} = \mathbf{J} \begin{bmatrix} \delta E \\ \delta c \end{bmatrix} \tag{25}$$

Equation 25 describes the time evolution of the small perturbations $\delta E = E - E_{ss}$ and $\delta c_s = c_s - c_{ss}$ of the given steady state through the Jacobian matrix. The elements of this matrix originate from the linear terms of the Taylor series expansions of the right-hand-sides of eqs 20, 21 around the steady-state values E_{ss} and c_{ss}

$$\mathbf{J} = \begin{bmatrix} \left(\dfrac{\partial F}{\partial E}\right)_{ss} & \left(\dfrac{\partial F}{\partial c_s}\right)_{ss} \\ \left(\dfrac{\partial G}{\partial E}\right)_{ss} & \left(\dfrac{\partial G}{\partial c_s}\right)_{ss} \end{bmatrix} =$$

$$\begin{bmatrix} \dfrac{-1}{2\pi r R_s C_d l_{max}} - \dfrac{v}{l_{max}} + \dfrac{nFc_{ss}}{C_d}\left(\dfrac{dk_f}{dE}\right)_{ss} & \dfrac{nFk_f(E_{ss})}{C_d} \\ -\dfrac{2c_{ss}}{\bar{\delta}_N}\left(\dfrac{dk_f}{dE}\right)_{ss} & -\dfrac{2k_f(E_{ss})}{\bar{\delta}_N} - \dfrac{2D_{ox}}{\bar{\delta}_N^{\,2}} \end{bmatrix} \tag{26}$$

According to the principles of the two-dimensional linear stability analysis, the nature of bifurcation, the given steady-state undergoes, is determined by the signs of the trace Tr and of the determinant Det of matrix $\mathbf{J}$

$$Tr = \frac{-1}{2\pi r R_s C_d l_{max}} - \frac{v}{l_{max}} + \frac{nFc_{ss}}{C_d}\left(\frac{dk_f}{dE}\right)_{ss} - \frac{2k_f(E_{ss})}{\bar{\delta}_N} - \frac{2D_{ox}}{\bar{\delta}_N^{\,2}} \tag{27}$$

$$Det = \left[\frac{-1}{2\pi r R_s C_d l_{max}} - \frac{v}{l_{max}} + \frac{nFc_{ss}}{C_d}\left(\frac{dk_f}{dE}\right)_{ss}\right]\left[-\frac{2k_f}{\bar{\delta}_N} - \frac{2D_{ox}}{\bar{\delta}_N^{\,2}}\right] + \left[\frac{nFk_f(E_{ss})}{C_d}\right]\left[\frac{2c_{ss}}{\bar{\delta}_N}\left(\frac{dk_f}{dE}\right)_{ss}\right] \tag{28}$$

where the derivative dk_f/dE is given by the formula

$$\left(\frac{dk_f}{dE}\right)_{ss} = \frac{-(\alpha n)_1 f k_{s,1}^{app} \exp[-(\alpha n)_1 f(E_{ss} - E_f^0)]}{1 + \exp[P_1(E_{ss} - P_2)]} - \frac{P_1 \exp[P_1(E_{ss} - P_2)] k_{s,1}^{app} \exp[-(\alpha n)_1 f(E_{ss} - E_f^0)]}{\{1 + \exp[P_1(E_{ss} - P_2)]\}^2} - (\alpha n)_2 f k_{s,2}^{app} \exp[-(\alpha n)_2 f(E_{ss} - E_f^0)] \tag{29}$$

For such parameters that $Det = 0$ the saddle-node (SN) bifurcation occurs, while $Tr = 0$ and $Det > 0$ are the conditions for the Hopf bifurcation (i.e., the onset of limit cycle oscillations from the single steady-state).[17−21]

In our calculation procedure, for a given voltage U and serial resistance R_s, first all the possible (1 to 3) steady-state potentials

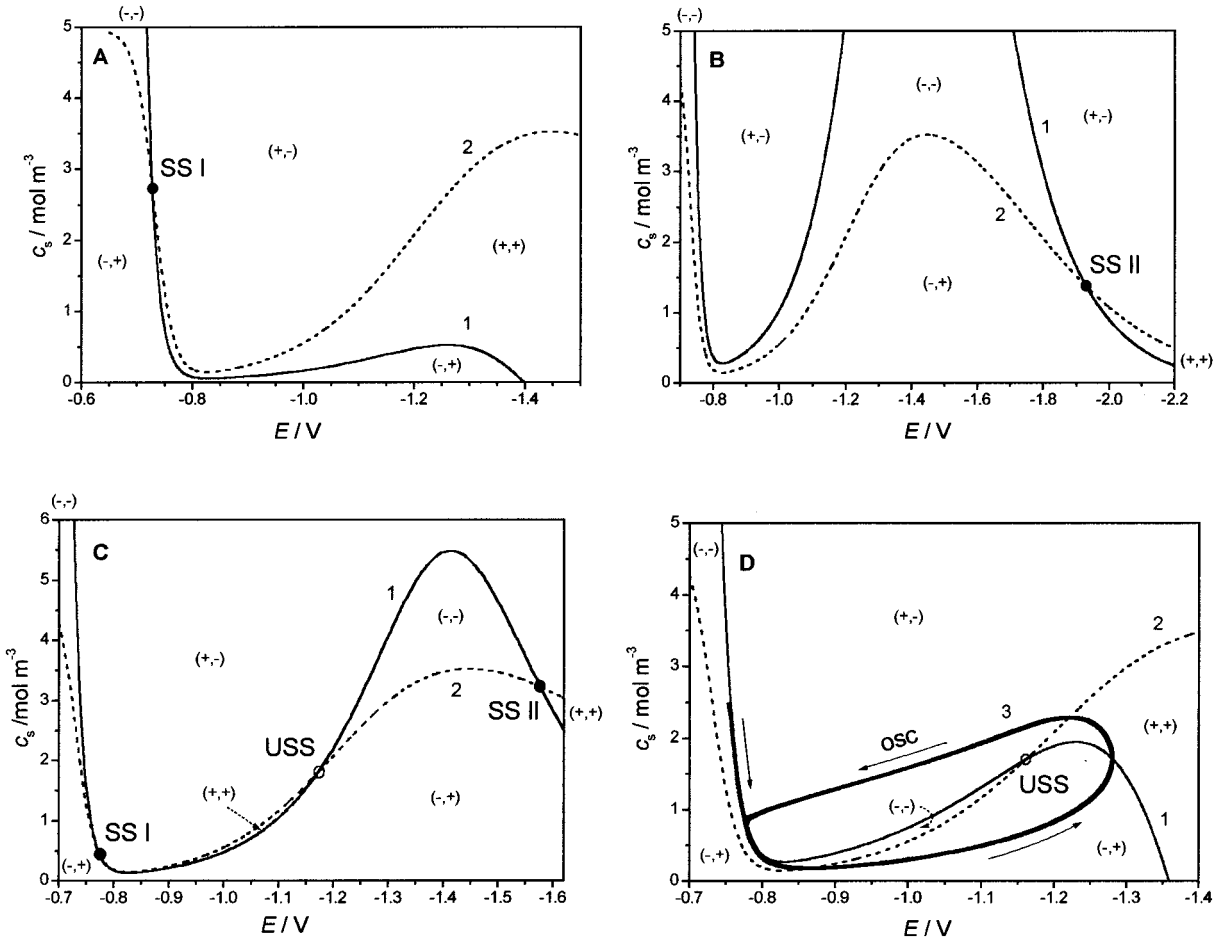

Figure 5. Analysis of steady-states (fixed points) of the differential eqs 20 and 21 in terms of the dE/dt nullcline (eq 23, curve 1) and dc_s/dt nullcline (eq 24, curve 2); (A) stable steady-state SS I (●, $E_{ss} = -0.728$ V; $c_{ss} = 2.727$ mol m^{-3}) for $U = -2$ V, $R_s = 6.0$ kΩ, (B) stable steady-state SS II (●, $E_{ss} = -1.930$ V; $c_{ss} = 1.381$ mol m^{-3}) for $U = -3.5$ V, $R_s = 3.0$ kΩ, (**C**) bistability SS I (●, $E_{ss} = -0.776$ V; $c_{ss} = 0.410$ mol m^{-3}) /SS II (●, $E_{ss} = -1.578$ V; $c_{ss} = 3.216$ mol m^{-3}) with medium unstable steady-state SS III (○, $E_{ss} = -1.172$ V; $c_{ss} = 1.795$ mol m^{-3}) for $U = -3.2$ V, $R_s = 5.5$ kΩ, (**D**) unstable steady-state USS (○, $E_{ss} = -1.162$ V; $c_{ss} = 1.694$ mol m^{-3}) for $U = -1.425$ V, $R_s = 0.7$ kΩ, surrounded by the stable limit cycle (curve 3), corresponding to sustained oscillations. The symbols in brackets, e.g., (+,−) denote the signs of the dE/dt and dc_s/dt derivatives in the appropriate regions of the plots, indicating the stability or instability of the steady-state considered.

E_{ss} were found numerically (using the bisection method) as the roots of the eq

$$\frac{U - E_{ss}}{2\pi r R_s C_d l_{max}} - \frac{(E_{ss} - E_{pzc})\upsilon}{l_{max}} + \frac{nFk_f(E_{ss})c^0_{ox} D_{ox}}{C_d[D_{ox} + k_f(E_{ss})\bar{\delta}_N]} = 0 \quad (30)$$

that comes from the combination of eqs 20 and 21 with the simultaneously imposed steady-state (fixed point) condition dE/dt = dc_s/dt = 0. The corresponding steady-state surface concentration c_{ss} is then calculated from eq 24 with $E = E_{ss}$. For these steady-state values, the corresponding determinant *Det* and the trace *Tr* of the Jacobian matrix were calculated. Repeating of this procedure for the set of values of U and R_s allows us to determine the position of points corresponding to the saddle-node and Hopf bifurcations. Such a theoretical diagram is presented in Figure 6-A. Beyond the small loop encircling the oscillatory region, other points of the Hopf bifurcations are located quite closely to the points of the saddle-node bifurcations, but these two courses do not collide in the (U, R_s) parameter range considered.

For comparison, Figure 6-B shows an analogous *experimental* bifurcation diagram, containing our previously published data.[9]

It is noteworthy that the theoretical diagram is similar to the experimental one. The following small differences can be reported: (i) the tiny region of oscillations, encircled by the points of the Hopf bifurcation, is slightly larger in the theoretical model (which fact presumably is caused by the simplification of the concentration profile by the strictly linear course, as suggested above), and (ii) the voltage region corresponding to the bistable behavior is slightly narrower in the theoretical than that in the experimental diagram. Nevertheless, the concordance between these two diagrams is good enough to prove the general validity of the presented theoretical analysis of the stability of steady-states at the streaming electrode.

Finally, both diagrams from Figure 6 qualitatively resemble the shape of the diagram of the interrelated oscillations and bistability, proposed by the Boissonade and De Kepper[1,26] for the description of a large class of nonelectrochemical dynamical systems. The universality of such dynamical nonlinear instabilities observed for completely different systems is thus again indicated. One can also note that if we invoke theoretical considerations of Guckenheimer,[27] we may suppose that the full detailed mathematical structure of the bifurcation scheme in Figure 6 is far more complex than our either experimental or theoretical analysis suggests. However, since these fine details seem to be actually unverifiable experimentally, in the present paper we limit the theoretical analysis to the points directly comparable with our currently available experimental data.

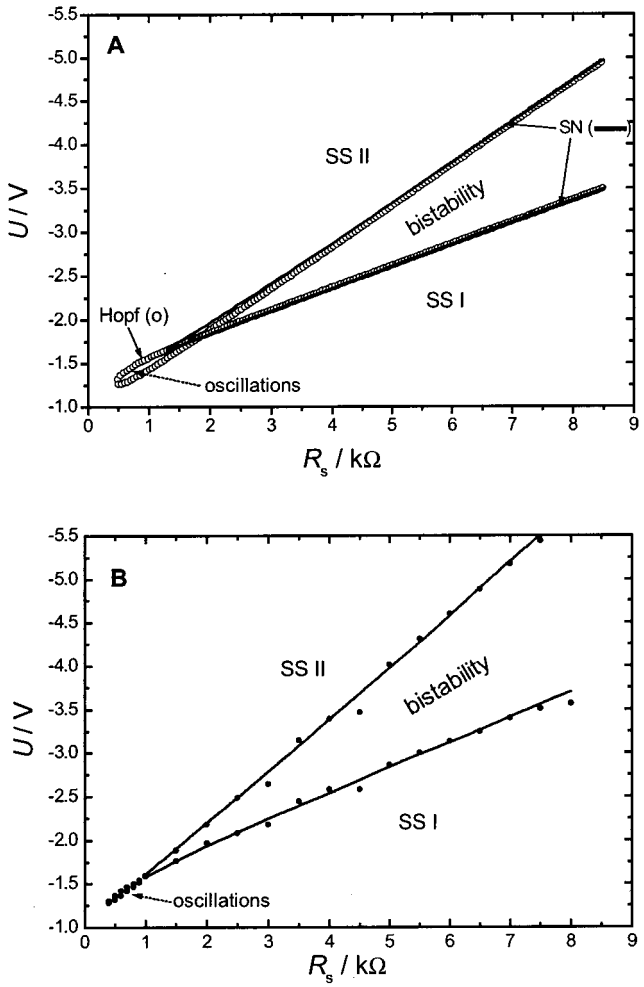

Figure 6. (A) Theoretical bifurcation diagram for the Ni(II)−SCN^- electroreduction, corresponding to the system of differential eqs 20 and 21, with $k_f(E)$ dependence given by eq 7: (—) points of the saddle-node bifurcation ($Det(\mathbf{J}) = 0$), (o) points of the Hopf bifurcation ($Tr(\mathbf{J}) = 0$ with $Det(\mathbf{J}) > 0$); (B) the corresponding experimental bifurcation diagram from ref 9.

Summary and Conclusions

The basic stability theory developed here for the streaming mercury electrode shows that it is possible to explain, at least semiquantitatively, the observed nonlinear dynamic behaviors in terms of relatively simple considerations. The analysis is based on the principal features of the (idealized) streaming electrode and on the theory of electrode processes controlled by the charge-transfer step, involving also the transport of the reactant from the bulk to the reaction site at the interface. Even the simplified forms of these equations, for which the linear stability analysis was applied, allows to construct the theoretical bifurcation diagram that exhibits distinct similarities to the experimentally found regions of oscillations and bistability. Thus, the approach described in this paper may be used for the prediction of the regions of instabilities in other systems studied at the streaming electrode. Also, for already studied systems it may appear helpful in the searches for eventual more complex behaviors, occurring in such a narrow region of control parameters that they are difficult to experimental detection without certain a priori knowledge about their existence. Of course, for the prediction of chaos the model would have to be extended to at least a three-dimensional space of dynamical variables. Both the experimental and theoretical work will be continued in this direction.

We would like also to emphasize that the present work, together with our previous paper[9] on the instabilities in the Ni(II)−SCN^- electroreduction at the streaming mercury electrode constitutes the collection of different ways in which the same electrochemical dynamical system can be analyzed. We started from the experiments and then applied their numerical modeling with an explicit finite differences method, which allowed to reproduce precisely and in a realistic way the bistable behavior.[9] Now, instead of a purely numerical approach, we first analyzed the existence of steady states and their stability in terms of analytical expressions for the faradaic and capacitive currents at the streaming electrode. Next, by invoking the principles of the linear stability theory for the equation of charge balance of the equivalent circuit, we found the specific instability condition for the steady-states at the streaming electrode. Third, we applied the formalism and standard techniques of linear stability analysis in two-dimensional (E, c_s) variable space for the construction of the bifurcation diagram. Such different treatments of the same problem allow to understand the processes underlying the occurrence of instabilities better than any of these approaches applied alone.

6. Appendix

Stability Analysis with Dimensionless Variables. In the present paper, the electrochemical system's dynamics for the streaming electrode has been analyzed in terms of real variables, for easy and direct comparison of our theoretical conclusions with the experimental results for the Ni(II)−SCN^- electroreduction. However, for a more general treatment of this type of the problem, it is also useful to transform the above-given equations to the corresponding *dimensionless* forms, according to typical methodology (cf. e.g., refs 21 and 28). Let us define the following dimensionless quantities

$$\text{electrode potential: } e = \frac{nF}{RT}E \tag{A1}$$

$$\text{externally applied voltage: } u = \frac{nF}{RT}U \tag{A2}$$

$$\text{time: } \tau = \frac{2D_{ox}}{\bar{\delta}_N^{\,2}}t \tag{A3}$$

$$\text{surface concentration: } \chi = \frac{c_{ox}(0,t)}{c_{ox}^0} \tag{A4}$$

Then, eqs 20 and 21 can be transformed to the following relationships, respectively

$$\epsilon\left(\frac{de}{d\tau}\right) = \frac{u-e}{\rho} - \frac{e-e_{pzc}}{\sigma} + k'\chi \tag{A5}$$

$$\frac{d\chi}{d\tau} = (1-\chi) - k'\chi \tag{A6}$$

with the dimensionless parameters, the values of which correspond to our experimental characteristics of the Ni(II)-SCN^-

electroreduction

$$\epsilon = \frac{2RTC_d}{n^2F^2 c_{ox}^0 \overline{\delta_N}} \cong 6 \times 10^{-3} \quad \text{(A7)}$$

$$\rho = \frac{2\pi n^2F^2D_{ox}c_{ox}^0 r l_{max}}{RT\overline{\delta_N}} \times R_s \cong 0.0368 \times R_s\,[\Omega] \quad \text{(A8)}$$

$$\sigma = \frac{n^2F^2D_{ox}c_{ox}^0 l_{max}}{RTv\overline{\delta_N}} \times \frac{1}{C_d} = \frac{2\pi r n^2F^2D_{ox}c_{ox}^0 l_{max}}{RT\overline{\delta_N}} \times$$

$$R_d \cong 65.49/C_d\,[\mathrm{F\ m^{-2}}] = 245.28 \quad \text{(A9)}$$

$$k' = \frac{\bar{\delta}_N}{D_{ox}} k_f \cong 1764.71 \times k_f\,[\mathrm{m\ s^{-1}}] \quad \text{(A10)}$$

Note that the difference in signs in eq A5, in comparison with analogous formulas for the nonstreaming electrodes in the literature (e.g., refs 21 and 28), is caused by our consequent assumption on the negative sign for the reduction current I_f, and for the working electrode potential E (and voltage U), expressed with respect to the appropriate reference electrode.

Such a transformation of the original eqs 20, 21 to their dimensionless forms (A5, A6) is particularly convenient for the discussion of the significance of the dimensionless parameter ϵ, equal here to ca. 0.006. This quantity determines the difference in the time scales of the dynamics of the electrode potential e (here, fast variable) and the surface concentration of the reactant χ (here, slower variable). However, it is noteworthy that the value of ϵ is actually for 1 to 2 orders of magnitude *higher* than that for the instabilities studied at the nonstreaming electrodes. An inspection of eq A7 shows that this is the consequence of a very short electrolysis time which determines the appropriately small diffusion layer thickness ($\bar{\delta}_N$) at the streaming electrode/electrolyte interface. Therefore, although for our experimental conditions the electrode potential E (or e) is still a relatively fast variable, it is not as fast as for the nonstreaming electrodes. Accordingly, the stable limit cycle trajectory (cf., Figure 5-d) is a rather smooth curve, without distinct straight-line sections, which means that the oscillations do *not* exhibit a typical relaxation shape, which fact is also concordant with our experimentally obtained oscillatory courses (see Figure 5 in ref 9).

References and Notes

(1) Field, R. J., Burger, M., Eds. *Oscillations and Travelling Waves in Chemical Systems*; Wiley-Interscience: New York, 1985.

(2) Gray, P.; Scott, S. K. *Chemical Oscillations and Instabilities*; Clarendon Press: Oxford, 1990.

(3) Orlik M. *Oscillating Reactions. Order and Chaos*; WNT: Warsaw, 1996 (in Polish).

(4) Kawczyński A. L. *Chemical Reactions − from Equilibrium, through Dissipative Structures, to Chaos*; WNT: Warsaw, 1990 (in Polish).

(5) Wójtowicz, J., In *Modern Aspects of Electrochemistry*; Bockris, J. O'M., Conway, B. E., Eds.; Plenum: New York, 1973; Vol. 8, p 47.

(6) Hudson J. L.; Tsotsis T. T. *Chem. Eng. Sci*. **1994**, *49*, 1493.

(7) Jurczakowski, R.; Orlik, M. *J. Electroanal. Chem*. **1999,** *478*, 118.

(8) Jurczakowski, R.; Orlik, M. *J. Electroanal. Chem*. **2000,** *486*, 65.

(9) Jurczakowski, R.; Orlik, M. *J. Phys. Chem. B,* **2002**, *106*, 1058.

(10) Jurczakowski, R.; Orlik, M., in preparation.

(11) Feldberg, S. W., In *Electroanalytical Chemistry*; Bard, A. J, Ed.; Marcel Dekker: New York 1969; Vol. 3, p 199.

(12) Britz, D. *Digital Simulation in Electrochemistry*, 2nd ed.; Springer: Berlin, 1988.

(13) Galus, Z. *Fundamentals of Electrochemical Analysis*, 2nd Ed.; Ellis Horwood/PWN: Chichester-Warsaw, 1994.

(14) Bard, A. J.; Faulkner, L. R. *Electrochemical Methods. Fundamentals and Applications*, 2nd Ed.; Wiley: New York, 2001.

(15) Weaver, J. R.; Parry, R. W. *J. Am. Chem. Soc*. **1956**, *78*, 5542.

(16) Weaver, R. J.; Parry, R. W. *J. Am. Chem. Soc*. **1954**, *76*, 6258.

(17) Ebeling, W. *Strukturbildung bei Irreversiblen Prozessen*; Teubner: Leipzig, 1976.

(18) Strogatz, S. H. *Nonlinear Dynamics and Chaos*; Addison-Wesley: Reading, MA, 1994.

(19) Schneider, F. W.; Münster, A. F. *Nichtlineare Dynamik in der Chemie*; Spektrum Akad. Vlg.: Heidelberg-Berlin-Oxford 1996.

(20) Kaplan D.; Glass L. *Understanding Nonlinear Dynamics*; Springer: New York 1995.

(21) Krischer K., In: *Modern Aspects of Electrochemistry, 32*; Bockris, J. O'M., Conway, B. E., White, R. E., Eds., Kluwer/Academic/Plenum Press: New York, 1999; p 1.

(22) Koper M. T. M. *Electrochim. Acta*, **1992**, *37*, 1771.

(23) Koryta, J. *Collect. Czech. Chem. Commun*. **1954**, *19*, 433.

(24) Koper, M. T. M.; Sluyters, J. H. *J. Electroanal. Chem.* **1991**, *303*, 73.

(25) Marciniak, A.; Gregulec, D., Kaczmarek, J. *Numerical Procedures in Turbo Pascal for Your PC*; Nakom: Poznań, 1991.

(26) Boissonade, J.; De Kepper, P. *J. Phys. Chem.* **1980**, *84*, 501.

(27) Guckenheimer, J. *Physica 20 D*, **1986**, 1.

(28) Koper, M. T. M., *Advanced Chemical Physics*; Prigogine I., Rice S. A., Eds.; Wiley: New York, 1996; Vol. XCII, p 161.